

# A NOVEL SHAPE-AWARE TOPOLOGICAL REPRESENTATION FOR GPR DATA WITH DNN INTEGRATION

MEIYAN KANG, SHIZUO KAJI, SANG-YUN LEE, TAEGLON KIM,  
HEE-HWAN RYU, AND SUYOUNG CHOI

**ABSTRACT.** Ground Penetrating Radar (GPR) is a widely used Non-Destructive Testing (NDT) technique for subsurface exploration, particularly in infrastructure inspection and maintenance. However, conventional interpretation methods are often limited by noise sensitivity and a lack of structural awareness. This study presents a novel framework that enhances the detection of underground utilities, especially pipelines, by integrating shape-aware topological features derived from B-scan GPR images using Topological Data Analysis (TDA), with the spatial detection capabilities of the YOLOv5 deep neural network (DNN). We propose a novel shape-aware topological representation that amplifies structural features in the input data, thereby improving the model's responsiveness to the geometrical features of buried objects. To address the scarcity of annotated real-world data, we employ a Sim2Real strategy that generates diverse and realistic synthetic datasets, effectively bridging the gap between simulated and real-world domains. Experimental results demonstrate significant improvements in mean Average Precision (mAP), validating the robustness and efficacy of our approach. This approach underscores the potential of TDA-enhanced learning in achieving reliable, real-time subsurface object detection, with broad applications in urban planning, safety inspection, and infrastructure management.

## 1. INTRODUCTION

Subsurface infrastructure inspection, particularly pipeline detection, is essential for the maintenance of urban environments [1], and it demands high-accuracy non-destructive testing (NDT) methods [2]. Ground Penetrating Radar (GPR) is a widely used geophysical technique for detecting and imaging subsurface structures in diverse fields such as archaeology, civil

---

*Date:* June 10, 2025.

*Key words and phrases.* Ground Penetrating Radar (GPR), Topological Data Analysis (TDA), Deep Neural Network (DNN), Object Detection, Sim2Real, Infrastructure Inspection, Pipeline Detection.

This research was supported by Basic Science Research Program through the National Research Foundation of Korea(NRF) (RS-2021-NR060141) and Korea Electric Power Corporation (R21SA02). The second author is partially supported by JST Moonshot R&D Grant Number JPMJMS2021 and the commissioned research (No.22301) by NICT, Japan.

engineering, and environmental studies [3, 4]. It works by emitting electromagnetic waves into the ground and analyzing the reflections to infer subsurface compositions.

Traditionally, GPR signal interpretation has relied on manual analysis and physics-based models, both of which are time-consuming, labor-intensive, susceptible to noise and sensitive to environmental variability. To overcome these limitations, recent efforts have increasingly turned to deep learning techniques for automating GPR data analysis. Among these, object detection models such as YOLO (You Only Look Once) [5], Faster R-CNN [6], and U-Net [7] have shown significant promise in improving detection accuracy and efficiency. YOLO models offer real-time object detection, enabling rapid classification of subsurface anomalies such as pipelines and voids, with minimal post-processing. Faster R-CNN typically provides higher accuracy, especially for small or low-contrast objects, but requires greater computational cost, limiting its suitability for real-time application [8]. U-Net excels at pixel-level segmentation, making it effective for complex subsurface delineation, though it can suffer from overfitting when training data is scarce.

Beyond individual model architecture, recent studies have explored more integrated framework for GPR interpretation. For instance, Lei et al. [9] proposed combining deep learning with reverse time migration, improving localization accuracy. Similarly, Su et al. [10] introduced an end-to-end framework tailored for underground utility detection, achieving promising results in real-world datasets.

Despite these advances, a key limitation persists: the performance of deep learning models is heavily reliant on the availability and diversity of high-quality annotated data. Collecting labeled GPR datasets is expensive and logistically challenging, prompting increased interest in simulation-based training approaches.

Sim-to-Real (Sim2Real) transfer has emerged as a viable solution by enabling models trained on simulated GPR data to generalize to real-world environments [11, 12]. Simulated environments allow for the generation of diverse, labeled, and noise-controlled data representing various subsurface conditions. These approaches help bridge the domain gap between synthetic and field data, improving model generalization and robustness.

Another promising direction lies in improving feature representation. Topological Data Analysis (TDA) provides a mathematical framework that captures intrinsic structural patterns often overlooked by conventional methods [13, 14]. TDA is particularly appealing in GPR analysis due to its invariance to coordinate transformations and robustness to noise [15, 16]. Its core technique, persistent homology, encodes the birth and death of topological features across multiple scales, producing a compact yet expressive representation of data geometry [17]. While prior studies typically use vectorized TDA outputs such as barcodes or persistence diagrams as features for machine learning, we proposed a different approach. In this work, we directly integrate topological features obtained from persistent homology with

raw B-scan GPR data. This fusion enables the model to learn both spatial textures and underlying shape structures, resulting in more informative representations and improved detection outcomes.

We introduce a deep learning framework that incorporates both Sim2Real training and TDA-based feature augmentation within a YOLOv5 pipeline. Our method demonstrates improved detection performance, as measured by mean Average Precision(mAP), and offers a robust, scalable solution for real-time subsurface object detection.

The remainder of this paper is organized as follows. Section 2 introduces the fundamental concepts of persistent homology, which serves as the core technique of this study. Section 3 describes the proposed framework, including the overall methodology and implementation details. Section 4 presents the experimental setup and reports the results based on the selected datasets.

## 2. PERSISTENT HOMOLOGY

*Topological Data Analysis (TDA)* is a mathematical framework that utilizes tools from algebraic topology to extract robust structural features from data, emphasizing the intrinsic *shape* of information [18].

One of the fundamental concepts in TDA is the homology of simplicial complexes or cubical complexes, which characterizes the topological properties of data [13]. A *cubical complex* is a type of topological space constructed by gluing together cubes of various dimensions in a structured way. Each cube is of the form  $[0, 1]^n$ , where  $n$  denotes the dimension, and the gluing is performed along faces of these cubes via isometries. For a collection of cubes to form a cubical complex, it must be closed under taking faces, and any intersection of two cubes in the complex must itself be a face of both. See [19] for details. Cubical complexes are particularly well suited for representing high-dimensional data structured on Cartesian grids, such as digital images. In comparison to simplicial complexes, they often provide a more natural and efficient framework for encoding such data. Such cubical complexes serve as foundational structures within TDA, allowing us to assign algebraic invariants such as homology groups. Roughly speaking, the ranks of these homology groups quantify essential topological features, including connected components ( $\beta_0$ ), loops or holes ( $\beta_1$ ), and higher-dimensional voids ( $\beta_2$ ).

The core technique within TDA for capturing multi-scale topological features is known as the *persistent homology* [20]. Persistent homology systematically tracks how homology groups evolve across multiple scales by examining a nested sequence of simplicial complexes, known as a *filtration*. Specifically, as the scale parameter changes, simplices are incrementally added to construct an increasing sequence of simplicial complexes. Persistent homology then records when topological features such as loops or voids appear (*birth*) and disappear (*death*) along this filtration.

As the scale  $\epsilon$  increases, a simplex is added whenever the discs (circles) of radius  $\epsilon$  around each set of vertices mutually intersect. We track the changes in the homology ranks as new simplices appear.

On the other hand, as the scale parameter  $\epsilon$  continues to increase and reaches another critical value  $d_2$ , the discs around the four vertices simultaneously intersect, causing triangles (two simplices) to fill the previously formed loop. Consequently, the loop disappears, reducing  $\beta_1$  back to 0. The scale interval during which a topological feature  $\sigma$ , such as a loop, is created (Birth( $\sigma$ )) and subsequently destroyed (Death( $\sigma$ )) is referred to as the *lifetime* (Lifetime( $\sigma$ )) of that feature:

$$(1) \quad \text{Lifetime}(\sigma) = \text{Death}(\sigma) - \text{Birth}(\sigma)$$

The length of this lifetime provides insight into the persistence and significance of topological structures within the datasets. Topological features with long lifetimes are likely to represent significant structures in the data, while short-lived features are often regarded as noise.

### 3. METHODOLOGY

The aim of this study is to accurately detect underground pipelines using *Ground Penetrating Radar* (GPR). In particular, we focus on analyzing B-scan images, which are the primary output of GPR measurements. A B-scan represents a two-dimensional cross-sectional image generated by sweeping the radar antenna along a linear path. Although B-scan images provide valuable information about subsurface structures, they are often contaminated with noise and clutter, making automated interpretation a challenging task.

To address this issue, we propose using TDA to enhance detection performance by extracting robust, noise-resistant features that capture the emphasize the inherent shape of the data. Specifically, we capture topological structures embedded in B-scan images, such as loops formed by hyperbolic reflections from buried cylindrical objects. These shape-aware topological features are then fused with the original image data, resulting in enriched structural representations that enhance the model's sensitivity to object geometry.

**3.1. Step 1: Shape-Aware Topological Representation.** The core contribution of this study lies in the extraction of topological features directly from image data. While TDA is typically effective when applied to datasets composed of isolated points, such as point clouds, it is not immediately compatible with structured data like images. Since images do not naturally form point clouds, conventional TDA tools such as the Vietoris-Rips complex cannot be directly applied.

To overcome this limitation, we develop a method for constructing filtered complexes from image data by introducing a scale parameter. This allows

us to adapt the principles of TDA to the image domain, enabling persistent homology to be computed meaningfully. Designing an appropriate filtration strategy for image-based data is thus a central technical contribution of this work.

Several studies have explored how TDA can be applied to image data; we refer the reader to relevant works for further background and methodologies [21, 22]. However, directly applying these approaches to GPR B-scan images is not straightforward due to the unique characteristics of GPR data. In particular, GPR images often contain high levels of clutter and noise, and the target features of buried pipelines appear as smooth, curved patterns rather than isolated, distinct shapes.

These differences motivate the need for a tailored approach that can effectively capture the topological signatures of subsurface objects in GPR imagery. In this work, we develop a new method for constructing filtered complexes suited to the characteristics of GPR data, enabling persistent homology to extract meaningful one-dimensional homological features ( $H_1$ ) that correspond to loop-like structures caused by hyperbolic reflections.

In this approach, images are processed through persistent homology using the following methods. The grayscale image is interpreted as a collection of individual pixels, where each pixel has an associated intensity value. This allows the image to be treated as a discrete set of data points embedded in a two dimensional grid, with pixel intensity serving as a scalar function defined over the domain. The image is represented as a cubical complex, where the filtration is constructed by varying intensity thresholds. As the threshold  $\epsilon$  increases, pixels with intensity less than or equal to  $\epsilon$  are included in the complex. These pixels naturally form connected structures in the form of cubical complexes, and we denote the resulting complex as  $K_\epsilon$ . For two thresholds  $\epsilon_1 < \epsilon_2$ , we have  $K_{\epsilon_1} \subseteq K_{\epsilon_2}$ , which implies that the sequence  $\{K_\epsilon\}_{\epsilon \geq 0}$  forms a filtered complex. The threshold  $\epsilon$  thus plays the role of a scale parameter in persistent homology; see Figure 1 for example.

Now, we focus exclusively on loops that emerge from the filtered complex, as our primary interest lies in the crescent-shaped closed patterns that represent subsurface pipelines. As the threshold  $\epsilon$  increases, we track the birth and death of one dimensional homology generators in the persistent homology of the filtered complex. Specifically, we record the intensity value at which each generator appears (birth) and the value at which it disappears (death).

Generators that persist over a wide range of thresholds are considered more significant, since longer lifetimes indicate greater topological relevance. In our analysis, we utilize the lifetime of each  $H_1$  generator as a key feature for detecting and interpreting meaningful structures in GPR images.

Persistent homology has become a powerful tool in data analysis, with persistence diagrams and barcodes serving as compact visual summaries of

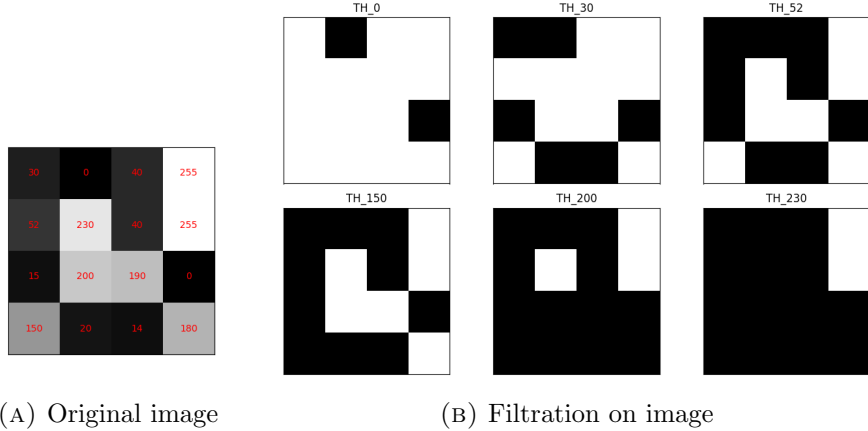


FIGURE 1. (a) Original image and (b) its filtration process.

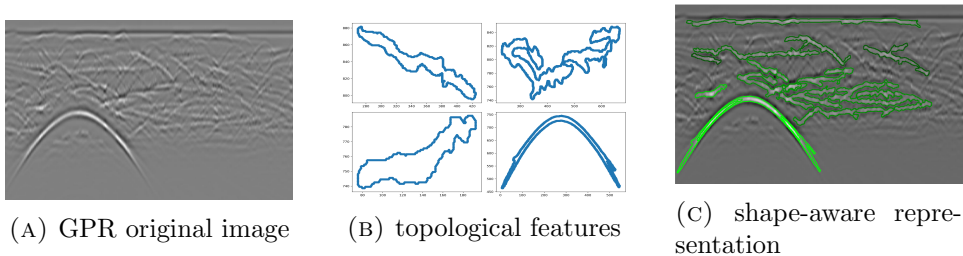


FIGURE 2. (a) Original GPR image and (b) Topological feature of GPR image (c) life-time weighted shape-aware representation of GPR image.

topological features across multiple scales. These conventional representations emphasize the timing of feature births and deaths. For object detection tasks, simply visualizing the birth and death of topological features is often insufficient. These events offer a coarse summary, but they do not capture the persistence and structural significance of features within the spatial domain. In contrast, our approach pivots to a different aspect: the lifetime of features—previously introduced in Equation 1. Hence, to incorporate the lifetime information into our analysis, we construct a new image with the same dimensions as the original input. In this image, we visualize the shapes of the degree one homology generators, modulating their *intensity* according to their lifetime. Generators with longer lifetimes are drawn with higher intensity, while those with shorter lifetimes appear with lighter shading. That offering a complementary perspective that deepens interpretability and uncovers more nuanced topological insights. This represents a novel contribution that, to our knowledge, has not been addressed in prior research.

An example of such a visualization, constructed from real GPR B-scan data using the proposed method, is shown in Figure 2.

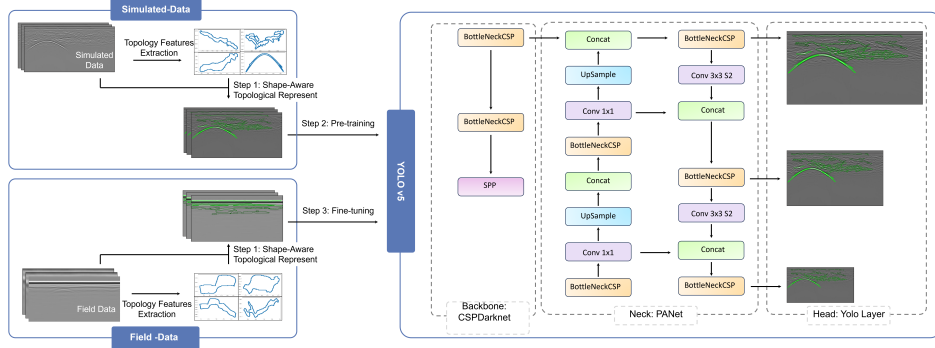


FIGURE 3. Our Framework: Step 1 – Topology feature extraction; Step 2 – Pre-train with simulated data; Step 3 – Fine-tune with field data.

**3.2. Step 2: Pre-training with TDA-Enhanced GPR Data.** Collecting and annotating real-world GPR data is labor-intensive and time-consuming, particularly in complex subsurface environments where buried utilities are difficult to access and label accurately. As a result, training YOLOv5 directly on large-scale field datasets is impractical. To address this limitation, we first pre-trained the model using a large set of synthetic GPR B-scan images generated with *gprMax*. The data generation procedure is described in detail in Section 4.1.

These simulated images are then processed through the TDA pipeline described in Section 3.1, where persistent  $H_1$  generators (e.g., loops formed by hyperbolic reflections) are extracted and encoded into lifetime-weighted shape-aware representations. These enhanced representations, illustrated in step 1 of Figure 3, capture structural patterns such as curvature and persistence, which are crucial for learning shape-based features associated with buried objects.

By training on this enriched synthetic data, the model can acquire generalized knowledge of subsurface patterns without requiring large annotated field datasets. However, simulated data alone cannot fully capture the complexity and variability of real-world environments. To mitigate this limitation, we adopt a Sim2Real strategy in which the pre-trained model is subsequently fine-tuned using a small set of annotated field scans.

**3.3. Step 3: Fine-tuning on YOLOv5 Using Field Data.** Following the pre-training phase, the model is fine-tuned using a curated set of real-world GPR scans obtained from a controlled testbed environment. These field data exhibit complex variations due to factors such as soil heterogeneity,

depth-dependent signal attenuation, and sensor-induced noise. The field data acquisition and experimental setup are detailed in Section 4.2.

To maintain consistency, these real-world B-scan images are processed using the same TDA-based pipeline introduced in Section 3.1, as shown in Step 1 of Figure 3. This ensures that both synthetic and field inputs are encoded in a topologically enriched, shape-aware format before being passed to the detection model.

Fine-tuning on field data is essential for bridging the domain gap between the idealized conditions of synthetic simulations and the stochastic, site-specific nature of real-world measurements. While pre-training enables the model to learn generalized geometric and topological priors, fine-tuning refines the learned parameters to adapt to real-world complexity.

This process enhances the model’s robustness and adaptability, allowing it to detect nuanced subsurface features more effectively. By incorporating a diverse range of field samples, the fine-tuning phase significantly improves real-world performance, enabling reliable detection of buried utilities under challenging and variable environmental conditions.

This two-stage training approach helps bridge the domain gap between synthetic and real data, improves robustness in unseen environments, and reduces the risk of overfitting.

#### 4. EXPERIMENTS AND RESULTS

**4.1. Numerical Data Generation.** We employed the Finite-Difference Time-Domain (FDTD) method, which discretizes time and space to numerically solve Maxwell’s equations, enabling accurate simulation of electromagnetic wave propagation. For this purpose, we used the open-source software *gprMax*, which allows efficient modeling of complex subsurface environments [23].

The simulation setup included essential components such as pipe placement, soil layering, and grid resolution to reflect realistic underground environments. A Ricker wavelet with a 350 MHz center frequency was used as the excitation signal. The radar system was modeled with a transmitter-receiver pair moved in 0.024 m increments, resulting in a total of 456 A-scans per simulation.

To specify ground material properties, we adopted the Peplinski model [24], which accounts for variables such as soil moisture and particle density. For greater realism, heterogeneous soil conditions were incorporated using a + fractal-based stochastic generation algorithm [25], which spatially distributes material properties in a self-similar pattern. In contrast, the homogeneous scenarios assumed constant permittivity values based on averaged water content.

Table 1 summarizes the key parameters used in the simulation. Pipe diameters ranged from 0.3 m to 1.0 m, with horizontal positions between 5.0 m and 11.0 m, and burial depths ranging between 3.5 m and 5.3 m.

Absorbing boundary conditions were applied on all sides with cell padding of [300, 300, 100, 150], corresponding to 1.8, m (left and right), 0.6, m (top), and 0.9, m (bottom), based on the grid resolution of 6, mm.

B-scan images were generated through 2D electromagnetic simulations under both homogeneous and heterogeneous conditions, with scenarios with single and multiple pipes. As shown in Figure 4, wave reflections vary depending on the complexity of subsurface configuration. To improve visibility of deep-layer structures, additional signal post-processing techniques were applied. To further improve the quality of the simulated GPR signals, we applied several signal processing techniques, including background removal (to eliminate static noise), band-pass filtering (to isolate the relevant frequency range), and Automatic Gain Control (AGC) for contrast normalization. The band-pass filter was applied in the frequency range of 100 MHz to 1900 MHz to retain informative signal components while suppressing irrelevant noise. For each B-scan image, five AGC variants were generated to increase the model’s robustness against intensity variations. In total, 1,200 simulated B-scan images were produced. An example output is shown in Figure 4(a).

TABLE 1. Modeling input properties for *gprMax* simulations

Category	Parameter	Value
Transmission	Wave type	Ricker
	Center frequency ( $f$ )	350 MHz
	A-Scan steps ( $n_{\text{step}}$ )	456
	Step-wise movement ( $\Delta l_{\text{step}}$ )	0.024 m/step
Model Geometry	Model size ( $W \times H$ )	16.0 m $\times$ 6.0 m
	Pipe diameter ( $D$ )	[0.3, 0.5, 1.0] m
	Pipe center ( $x_c, y_c$ )	([5.0–11.0] m, [3.5–5.3] m)
Grid	Cell size ( $\Delta l$ )	6 mm
Boundary	Absorbing BC ( $BC$ )	[1.8, 1.8, 0.6, 0.9] m

**4.2. Field Data Collection.** Real-world GPR data were collected from a controlled testbed located in Gapyeong and at Daragjae-ro 451, Seorak-myeon, Gapyeong-gun, Gyeonggi-do, South Korea. The experimental sites were designed to emulate realistic subsurface conditions, including multiple buried pipelines at varying depths and orientations.

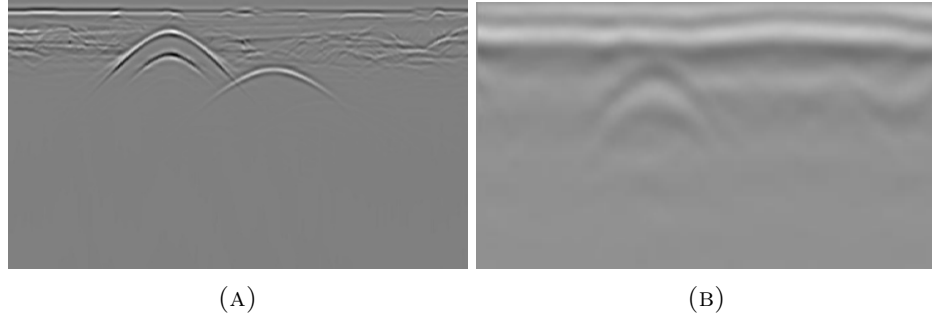


FIGURE 4. B-Scan samples in Fig. 2: (a) simulated sample data; (b) real world sample data.

Figure 5 illustrates the layout of the test environment, highlighting the spatial configuration of buried targets, soil composition, and surface accessibility. The testbeds provide a semi-controlled setting that balances experimental repeatability with real-world variability. Different types of subsurface objects, such as corrugated pipes, hume pipes, cast iron pipes, and drainpipes, were installed at known locations and depths. Seven scanning paths (Lines 1–7) were used to acquire B-scan images under varying subsurface configurations.

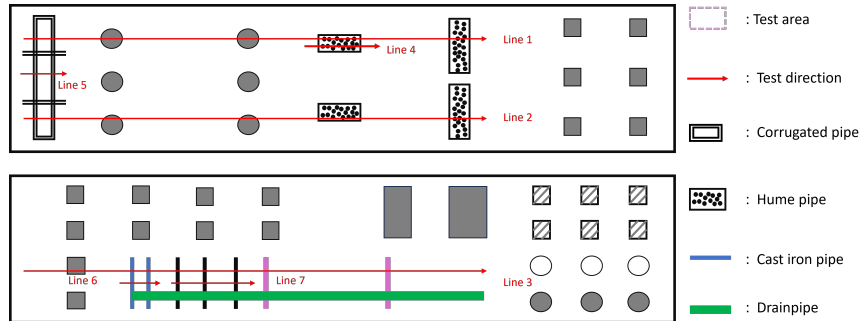


FIGURE 5. Field data collection sites

Field data were collected using a commercial GPR system developed by Systems, Inc. (USA). The system consisted of a main control unit (*SIR 4000*), a 350 MHz antenna (*Model 350HS*), and a survey cart equipped with an encoder wheel (*Model 653*). The antenna frequency offered a balanced trade-off between resolution and penetration depth. The encoder-enabled survey cart enabled precise distance measurements during data scanning. All components were integrated into a single mobile platform for efficient field deployment. The acquired B-scan signals were post-processed using *Radan 7* software on a standard PC to enhance featured visibility and interpretability. Standard signal processing procedures were applied, including

background removal, band-pass filtering (centered around the 350, MHz antenna frequency), and time-varying gain adjustment. These procedures are consistent with those used in simulated data processing, enabling a fair comparison between simulated and real-world signals. A total of 106 real-world B-scan images were collected and used in the training pipeline. Figure 5(b) presents an example scan from the testbed.

**4.3. Results and Comparison.** To assess the effectiveness of shape-aware topological representation in improving object detection performance, we compare two model configurations:

- **Baseline:** A YOLOv5 model trained solely on raw GPR images, without any topological enhancement.
- **Proposed:** A YOLOv5 model trained on shape-aware representations generated via persistent homology.

A total of 1,306 B-scan images were used in this study, comprising 1,200 simulated and 106 real-world scans. Each dataset was independently split into training and validation sets, with 70% of the data used for training and 30% for validation. Specifically, 840 simulated and 74 real-world images were used for training, while the remaining 360 simulated and 32 real-world images were used for validation. This separation strategy ensured balanced representation and fair evaluation across both synthetic and real domains.

Both configurations followed a two-stage training procedure: initial pre-training on simulated data, followed by fine-tuning with real-world field scans. This consistent training protocol enabled us to isolate and evaluate the effect of topological integration on model performance.

The evaluation relies on standard object detection metrics, including *Precision*, *Recall*,  $mAP@0.5$ , and  $mAP@0.5:0.95$ . We also assess validation losses such as box loss and objectness loss, which reflect localization and object confidence, respectively. Although classification loss is computed internally by YOLOv5, it is excluded from our analysis due to the single-class nature of the detection task.

As shown in Table 2, the TDA-enhanced model consistently outperforms the baseline across all metrics. During pre-training, mAP scores improve while box loss remains comparable. During fine-tuning with field data, the proposed model shows further gains in detection accuracy and a reduction in box loss, highlighting its generalization capability and training efficiency.

Figure 6 (a) and (b) shows improved mAP scores at multiple IoU thresholds, while Figure 6 (c) and (d) highlights smoother and more stable trends in *precision* and *recall*. In addition, loss curves in Figure 6 (e) and (f) demonstrate that TDA-enhanced models yield lower error values with faster convergence. These results collectively indicate that integrating topological features improves detection robustness, enhances generalization, and facilitates more stable training, particularly under the variability of field-acquired data.

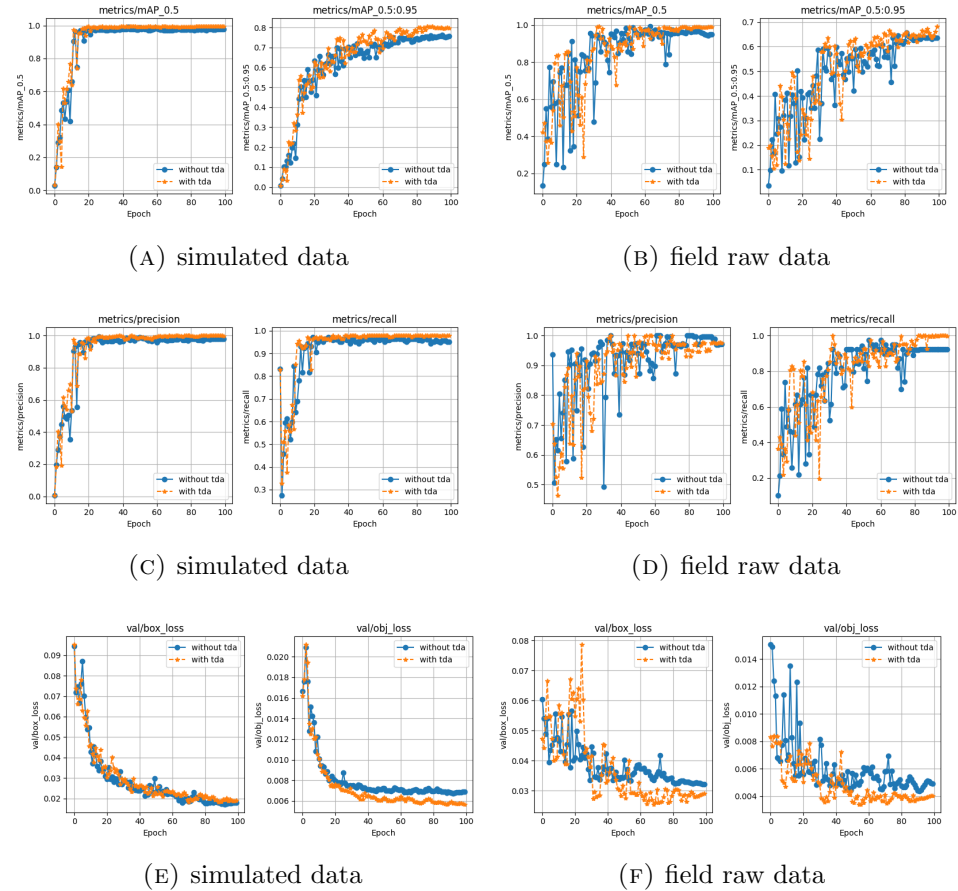


FIGURE 6. Map comparison with pre-trained stage and fine-tuned stage

TABLE 2. Impact of TDA on Model Performance

Process	Box Loss	mAP@0.5	mAP@0.5:0.95	TDA
Pretrained	0.017	0.975	0.757	No
	0.019	0.993	0.801	Yes
Fine Tuned	0.029	0.950	0.635	No
	0.023	0.988	0.682	Yes

## CONCLUSION

This study introduces a novel framework that integrates shape-aware topological representations with deep learning-based object detection in GPR data. By extracting persistent homology features and encoding them

as lifetime-weighted images, the model gains improved sensitivity to subsurface structural patterns that are often obscured in raw B-scan inputs. Experimental results confirm that the proposed TDA-enhanced YOLOv5 significantly improves detection accuracy, training stability, and generalization across both simulated and real-world datasets. These findings demonstrate the potential of topological feature integration in advancing GPR-based subsurface sensing. Future research will explore extensions to multi-class detection, unsupervised learning of topological priors, and broader validation across diverse geophysical conditions.

To ensure robustness across diverse data distributions, we adopted a Sim2Real training strategy comprising pre-training on synthetic GPR data and fine-tuning with real-world field scans. Experimental results confirmed that the proposed TDA-enhanced YOLOv5 model consistently improves detection accuracy, training stability, and generalization across both domains. Notably, even under the complex and noisy conditions of field environments, the model achieved higher mAP scores and lower localization errors compared to the baseline.

Overall, these findings demonstrate the potential of topological feature integration for advancing GPR-based sensing technologies. Future work will explore multi-class detection, unsupervised learning of topological priors, and deployment across a broader range of subsurface conditions.

## REFERENCES

- [1] G. Yang, D. Yuan, T. Xu, and B. Li, “An adaptive clutter-immune method for pipeline detection with gpr,” *IEEE Sensors Journal*, vol. 23, no. 19, pp. 22 984–22 997, 2023.
- [2] A. Neal, “Ground-penetrating radar and its use in sedimentology: principles, problems and progress,” *Earth-science reviews*, vol. 66, no. 3-4, pp. 261–330, 2004.
- [3] D. J. Daniels, *Ground penetrating radar*. Iet, 2004, vol. 1.
- [4] H. M. Jol, *Ground penetrating radar theory and applications*. elsevier, 2008.
- [5] J. Redmon, S. Divvala, R. Girshick, and A. Farhadi, “You only look once: Unified, real-time object detection,” in *Proceedings of the IEEE Conference on Computer Vision and Pattern Recognition (CVPR)*, 2016, pp. 779–788.
- [6] S. Ren, K. He, R. Girshick, and J. Sun, “Faster r-cnn: Towards real-time object detection with region proposal networks,” *IEEE transactions on pattern analysis and machine intelligence*, vol. 39, no. 6, pp. 1137–1149, 2016.
- [7] O. Ronneberger, P. Fischer, and T. Brox, “U-net: Convolutional networks for biomedical image segmentation,” in *Medical Image Computing and Computer-Assisted Intervention (MICCAI)*, 2015, pp. 234–241.
- [8] Z. Fang, Z. Shi, X. Wang, and W. Chen, “Roadbed defect detection from ground penetrating radar b-scan data using faster rcnn,” *IOP Conference Series: Earth and Environmental Science*, vol. 660, no. 1, p. 012020, feb 2021.
- [9] J. Lei, H. Fang, Y. Zhu, Z. Chen, X. Wang, B. Xue, M. Yang, and N. Wang, “Gpr detection localization of underground structures based on deep learning and reverse time migration,” *NDT & E International*, vol. 143, p. 103043, 2024.
- [10] Y. Su, J. Wang, D. Li, X. Wang, L. Hu, and Y. Kang, “End-to-end deep learning model for underground utilities localization using gpr,” *Automation in Construction*, vol. 149, p. 104776, 2023.

- [11] K. Raha and K. P. Ray, "Ground Penetrating Radar Model and its Validation using Developed Prototype," *Wireless Personal Communications*, vol. 135, no. 2, pp. 1233–1244, 2024.
- [12] G. Junkai, S. Huaifeng, S. Wei, L. Dong, Y. Yuhong, Z. Yi, L. Rui, and L. Shangbin, "Gpr-transunet: An improved transunet based on self-attention mechanism for ground penetrating radar inversion," *Journal of Applied Geophysics*, vol. 222, p. 105333, 2024.
- [13] H. Edelsbrunner and J. Harer, *Computational Topology: An Introduction*. American Mathematical Society, 2010.
- [14] R. Ghrist, "Barcodes: the persistent topology of data," *Bulletin of the American Mathematical Society*, vol. 45, no. 1, pp. 61–75, 2008.
- [15] P. Bubenik, "Statistical topological data analysis using persistence landscapes," *Journal of Machine Learning Research*, vol. 16, pp. 77–102, 2015.
- [16] L. Wasserman, "Topological data analysis," *Annual Review of Statistics and Its Application*, vol. 5, pp. 501–532, 2018.
- [17] F. Chazal and B. Michel, "An introduction to topological data analysis: Fundamental and practical aspects for data scientists," *Frontiers in Artificial Intelligence*, vol. 4, p. 667963, 2021.
- [18] G. Carlsson, "Topology and data," *Bulletin of the American Mathematical Society*, vol. 46, no. 2, pp. 255–308, 2009.
- [19] T. Kaczynski, K. Mischaikow, and M. Mrozek, *Computational homology*, ser. Applied Mathematical Sciences. Springer-Verlag, New York, 2004, vol. 157. [Online]. Available: <https://doi.org-ssl.openlink.ajou.ac.kr/10.1007/b97315>
- [20] D. Horak, S. Maletić, and M. Rajković, "Persistent homology of complex networks," *Journal of Statistical Mechanics: Theory and Experiment*, vol. 2009, no. 03, p. P03034, 2009.
- [21] A. Asaad, "Persistent homology for image analysis," Ph.D. dissertation, 01 2020.
- [22] D. A. Brito-Pacheco, C. C. Reyes-Aldasoro, and P. Giannopoulos, "Persistent homology in medical image processing: A literature review," *medRxiv*, pp. 2025–02, 2025.
- [23] C. Warren, A. Giannopoulos, and I. Giannakis, "gprmax: Open source software to simulate electromagnetic wave propagation for ground penetrating radar," *Computer Physics Communications*, vol. 209, pp. 163–170, 2016.
- [24] N. R. Peplinski, F. T. Ulaby, and M. C. Dobson, "Dielectric properties of soils in the 0.3-1.3-ghz range," *IEEE transactions on Geoscience and Remote sensing*, vol. 33, no. 3, pp. 803–807, 1995.
- [25] F. J. Molz, H. Rajaram, and S. Lu, "Stochastic fractal-based models of heterogeneity in subsurface hydrology: Origins, applications, limitations, and future research questions," *Reviews of Geophysics*, vol. 42, no. 1, 2004.

DEPARTMENT OF MATHEMATICS, AJOU UNIVERSITY, 206, WORLD CUP-RO, YEONGTONG-GU, SUWON 16499, REPUBLIC OF KOREA

*Email address:* miyeon@ajou.ac.kr

INSTITUTE OF MATHEMATICS FOR INDUSTRY, KYUSHU UNIVERSITY, FUKUOKA, 819-0395, JAPAN; GRADUATE SCHOOL OF SCIENCE, KYOTO UNIVERSITY, KYOTO, 606-8502, JAPAN

*Email address:* skaji@imi.kyushu-u.ac.jp

CONSTRUCTION ENVIRONMENT SYSTEM RESEARCH INSTITUTE, INHA UNIVERSITY, INCHEON, 22212, REPUBLIC OF KOREA

*Email address:* sangyunlee@kict.re.kr

DEPARTMENT OF MATHEMATICS, AJOU UNIVERSITY, 206, WORLD CUP-RO, YEONGTONG-GU, SUWON 16499, REPUBLIC OF KOREA

*Email address:* nayo6180@gmail.com

TRANSMISSION & SUBSTATION LABORATORY, KOREA ELECTRIC POWER CORPORATION (KEPCO) RESEARCH INSTITUTE, DAEJEON, 34056, REPUBLIC OF KOREA

*Email address:* hhryu82@kepc.co.kr

DEPARTMENT OF MATHEMATICS, AJOU UNIVERSITY, 206, WORLD CUP-RO, YEONGTONG-GU, SUWON 16499, REPUBLIC OF KOREA

*Email address:* schoi@ajou.ac.kr